Label-free and high-throughput removal of residual undifferentiated cells from iPSC-derived spinal-cord progenitor cells

Tan Dai Nguyen[1, †], Wai Hon Chooi,[3, †] Hyungkook Jeon, [2, 8, †] Jiahui Chen,[4] Daniel Ninio Roxby,[1,4] Jerome Tan,[1,4,7] Cheryl Yi-Pin Lee,[3] Shi-Yan Ng,[3] Jongyoon Han,[1,2, *] Sing Yian Chew,[4,5,6,*]

[1] Critical Analytics for Manufacturing of Personalized Medicine, Singapore-MIT Alliance for Research and Technology, 1 Create Way, #04-13/14, Singapore, 138602

[2] Department of Electrical Engineering and Computer Science & Department of Biological Engineering, Massachusetts Institute of Technology, 77 Massachusetts Ave, Cambridge, MA 02139, USA

[3] Institute of Molecular and Cell Biology, A*STAR Research Entities, 61 Biopolis Dr, Proteos, Singapore, 138673

[4] School of Chemical and Biomedical Engineering, Nanyang Technological University, 62 Nanyang Dr, Singapore, 637459

[5] School of Materials Science and Engineering, Nanyang Technological University, 50 Nanyang Ave, Singapore, 639798

[6] Lee Kong Chian School of Medicine, Nanyang Technological University, 59 Nanyang Drive, Singapore, 636921

[7] NTU Institute for Health Technologies, Interdisciplinary Graduate Programme, Nanyang Technological University, 61 Nanyang Dr, Singapore,637335

[8] Department of Manufacturing Systems and Design Engineering, Seoul National University of Science and Technology, 232 Gongneung-ro, Nowon-gu, Seoul 01811, the Republic of Korea

[†] These authors contributed equally to this work

* Corresponding author. Email addresses: SYChew@ntu.edu.sg (Sing Yian Chew), jyhan@mit.edu (Jongyoon Han), tandai@outlook.sg (Tan Dai Nguyen), Chooi_Wai_Hon@imcb.a-star.edu.sg (Wai Hon Chooi), hkjeon@seoultech.ac.kr (Hyungkook Jeon)

1. Abstract:

Spinal cord progenitor cells (SCPCs) have the capability to differentiate into multiple cell lineages of a central nervous system. The transplantation of SCPCs derived from human induced pluripotent stem cells (iPSCs) has beneficial effects on treating spinal cord injury (SCI). However, the presence of residual undifferentiated iPSCs amongst their differentiated progeny poses a high risk as it can result in the development of teratomas or other types of tumors post-transplantation. Despite the need to remove these residual undifferentiated iPSCs, there is a severe lack of surface markers that can identify them for subsequent removal. In this study, iPSCs were differentiated into SCPCs through a 10-day differentiation process. By profiling the size of SCPCs, we found that the large-sized group contains significantly more cells expressing pluripotent markers. A sized-based, label-free separation using an inertial microfluidic-based device was exploited to remove tumor-risk cells. The device takes advantage of label-free, non-contact, and high throughput (*i.e.,* > 3 million cells per minute) without affecting cell viability and functions. The sorted cells were verified with immunofluorescence staining, flow cytometry analysis, and colony culture assay. Essentially, our technology has demonstrated its capabilities to reduce the percentage of tumor-risk cells up to

98.07 %. Our technology has great potential for the 'downstream processing' of cell manufacturing workflow, contributing to better quality and safety of the transplanted cells.

1. Introduction:

Recent studies show that it is now possible to convert somatic cells into pluripotent stem cells that closely resemble embryonic stem cells – the induced pluripotent stem cell (iPSC) [1]. The autologous iPSCs that are derived from a patient's own somatic cells not only bypass many ethical issues but also solve the problem of immunological rejection. However, the tumorigenicity of iPSCs remains a big hurdle to overcome for safe therapeutic applications using iPSC-derived differentiated cells [2-5]. Sharing similar properties to human embryonic stem cells (hESCs) in terms of unlimited self-renewal and pluripotent, undifferentiated iPSCs could form mature teratomas in a dose-dependent manner [2, 6, 7]. Moreover, the iPSCs are likely to be more tumorigenic than hESCs, owing to their risk for the development of teratocarcinoma and possibly somatic tumors [8, 9]. The potential tumorigenicity risk of residual undifferentiated iPSCs is dependent on not only the number of undifferentiated iPSCs but also the features of the cell lines [3] and culture adaptation[10]. Hence, the tumorigenicity of iPSCs-derived differentiated cells should be evaluated for each cell line and each cell culture batch. Results from a preclinical tumorigenicity and biodistribution safety study that was required by the US Food and Drug Administration (FDA) and Australian Therapeutic Goods Administration (TGA) prior to conducting a Phase I clinical trial showed that the lack of residual undifferentiated cells (less than 0.001 %) had the negligible tumorigenic potential [11]. Moreover, a recent clinical trial of transplantation of iPSC-derived neural stem/progenitor cells in a model of spinal cord injury (SCI) used the expression of OCT4 for the detection of residual undifferentiated cells [12].

Removal methods of residual iPSCs or ESCs have been reported, including cytotoxic antibodies [13-15], fluorescence-activated cell sorting (FACS) [16-18], magnetic-activated cell sorting (MACS) [19, 20], small molecules [21, 22]. These methods rely heavily on the specific cell surface markers which lacks sufficient specificity for pluripotent cells. Alternative removal methods utilize gene manipulation or chemical inhibitor, which are not suitable for high-throughput cell therapy manufacturing.

It has been shown that transplantation of early-stage NSCs or progenitors resulted in the greatest neural tissue and functional repair compared to transplantation of more mature neurons and reduced the secondary tissue damage [23, 24]. Recently, several studies found that region-specific neural progenitors have better efficacy in terms of cell engraftment to treat spinal cord injury [25-27]. On other hand, cell-based therapies based on the immune-privileged Umbilical Cord

Lining Epithelial cells (CLECs)-derived iPSCs have a high potential to be developed into off-the-shelf clinical products due to their immunosuppressive properties [28, 29]. In this study, we used iPSCs derived from CLECs, which were then differentiated into Spinal-Cord Progenitor Cells (SCPCs) as the model system. A label-free and high-throughput microfluidic spiral sorter was developed to eliminate the residual undifferentiated cells from SCPC populations. Based on the quality control (QC) strategy of detecting OCT4-positive cells from a recent clinical trial of transplantation of iPSC-derived neural stem/progenitor cells in subacute complete spinal cord injury [12], expression of OCT4 was analyzed using immunostaining, flow cytometry, and colony culture assay [30], to quantify the purity of sorted cells.

2. Materials and methods

2.1. Spinal Cord Progenitor Cells (SCPCs) differentiation from human induced pluripotent stem cells (iPSCs)

CLEC-derived iPSCs were maintained in StemMACS iPS-Brew XF cell culture medium on Matrigel Matrix coating (Corning, New York, USA). The iPSCs were routinely passaged every 5-7 days using ReLeSR™ Passaging Reagent (Stemcell Technologies, Vancouver, Canada). The iPSCs were then differentiated towards SCPCs based on a modified protocol that was used to generate spinal motor neurons [31, 32]. Briefly, when the iPSCs were 70-80% confluent, the iPSCs were dissociated into single cell suspension using Accutase (Nacalai Tesque Inc., Kyoto, Japan). The dissociated iPSCs were then counted and reseeded at a density of 800,000 cells per well in a 6-well plate in a neural induction medium supplemented with ROCK inhibitor (5 µM). The neural induction medium consisted of DMEM/F12 (50 %, Biological Industries, Haemek, Israel), neural medium (50 %), NeuroBrew-21 (1X), N2 (1X), Non-Essential Amino Acid (1X, Thermo Fisher Scientific, Waltham, MA, USA), glutamax (0.5X, Thermo Fisher Scientific), LDN-193189 (0.5 µM), and CHIR-99021 (4.25 µM). On day 3, retinoic acid (RA, 10 µM, Sigma, St. Louis, MO, USA) was added to the medium. On day 4, the cells were reseeded at a lower density (2 million cells per 100 mm dish) in the same medium and maintained with regular medium change until day 10. On day 10, the cells were characterized and termed as SCPCs, which were then frozen or used for experiments. All other culture components were purchased from Miltenyi Biotech (Bergisch Gladbach, Germany) unless specified.

2.2. Microfluidic spiral sorted design and fabrication

The polydimethylsiloxane (PDMS) spiral sorter was fabricated via the standard soft-lithographic technique. 3D CAD software (SolidWorks 2020, Waltham, MA, USA) was used to design an aluminum mold for making the PDMS spiral sorter replica, and the aluminum mold was

fabricated via a micro-milling process (Whits Technologies, Singapore). Here, we used the multi-dimensional double spiral (MDDS) inertial microfluidic device as the spiral sorter [33-35], and its optimal channel dimensions and channel configuration were determined based on the observation of trajectories of particles having various sizes (7-30 µm) in the devices having different channel dimensions. The first spiral channel was designed to have a relatively smaller channel dimension to obtain a higher inertial lift force, resulting in the focusing of all the target particles or cells into the inner wall side of the channel whereas the second spiral channel has a relatively larger channel dimension so that particles can reach their different equilibrium locations determined by the balance between inertial lift and Dean drag forces, resulting in the sorting of the particles depending on their sizes. From the particle trajectory observation using multiple MDDS devices having different dimensions, we empirically selected an optimal MDDS device where the first spiral channel has a rectangular cross-section with 800 µm in width and 100 µm in height with three loops while the second channel has a trapezoidal cross-section with 800 µm in width and 120 and 180 µm in height for the inner- and outer-wall sides, respectively.

A 10:1 mixture of PDMS base and curing agent (Sylgard 184, Dow Corning, Inc.) was used to make the PDMS MDDS replica. After curing on the hot plate for 10 minutes at 80 °C, the PDMS MDDS replica was bonded to a glass substrate using a plasma machine (Femto Science, Korea).

2.3. SCPCs sorting using spiral sorter

Prior to the sorting, the spiral sorter was incubated with 70% ethanol for 30 minutes for sterilization and rinsed with 1X PBS and then medium. The cells were loaded into a 20 mL syringe before injecting into the device using a syringe pump (PHD ULTRA™ Syringe Pumps, Harvard Apparatus, Massachusetts, USA). For the recirculation strategy, a dual check valve (Quosina, New York, USA) was used to retract the sorted cells into the syringe based on the withdrawal motion of the syringe pump before resorting.

2.4. Immunofluorescent staining

The sorted cells were seeded at a density of 80,000 cells per well in a 96-well plate. After the cells were attached to the wells overnight, the cells were fixed in 4% paraformaldehyde (PFA) for 15 minutes at room temperature. Thereafter, the cells were permeabilized in 0.1% Triton X-100 for 15 minutes followed by 1 hour of incubation in the blocking buffer (5% FBS and 1%BSA in PBS) at room temperature. The cells were then incubated in primary antibodies diluted in the blocking buffer at 4 °C overnight. The primary antibodies used were: OCT4 (1:500, Santa Cruz Biotechnology sc-5279), SOX1 (1:500, Cell Signaling Technology 4194S), and HOXB4 (1:200,

Abcam ab133521). On the next day, the cells were washed with PBS and incubated in respective secondary antibodies (donkey anti-mouse AF 488/donkey anti-rabbit AF 568, 1:1000, Thermofisher) and DAPI diluted in blocking buffer (1:1000, Thermofisher) for 1 h at room temperature. The cells were then washed with PBS before imaging. Imaging was performed on a Leica DMi8 microscope or Opera Phenix High-Content Screening System using 10× or 20× objectives.

2.5. Flow cytometry analysis

Cells were collected in 15 mL centrifuge tubes and adjusted to 2×10^6 cells/tube. They were then fixed in 4% PFA and incubated at room temperature for 15 minutes. Thereafter, the fixed cells were pelleted by centrifugation at 3000 rpm for 5 minutes and washed once with PBS. Next, cells were stained by incubation at room temperature for at least 2 hours with a primary antibody in perm/block buffer (0.5% saponin, 1% BSA). The primary antibodies used were: OCT4 (1:500, Santa Cruz Biotechnology sc-5279), SOX1 (1:500, Cell Signaling Technology 4194S). Cells were centrifuged and washed twice with PBS. They were then stained by incubation in the dark at room temperature for at least 45 minutes with a second antibody in perm/block buffer. After that, they were washed with PBS and resuspended in PBS. Before running with the Cytoflex flow cytometer (Beckman Coulter, California, USA), cells were filtered through the 45 µm cell strainer to remove cell clumps and kept on ice. Compensation was performed and applied to the analysis.

2.6. EdU proliferation assay

SCPC and hiPSC proliferation was measured with the Click-iT EdU flow cytometry assay kit (Invitrogen). EdU (5-ethynyl-2′-deoxyuridine) is a nucleoside analog to thymidine and is incorporated into DNA during active DNA synthesis. The EdU was added (10 µM) to the culture medium before seeding for incubation. The incubation time was approximately 24 hours. Cells were then harvested, rinsed in PBS with 1% BSA, and removed supernatant. They were fixed with Click-iT fixative for 15 min in the dark at room temperature and rinsed in PBS with 1% BSA. Then, they were permeabilized with 1X Click-iT® saponin-based permeabilization for 15 min at room temperature in the dark. After that, they were incubated for 30 min at room temperature in the dark with a Click-iT reaction cocktail. Cells were washed and resuspended with 1X Click-iT® saponin-based permeabilization and wash reagent before being analyzed by Cytoflex flow cytometer (Beckman Coulter, California, USA).

2.7. Colony culture assay

Cells were seeded in a 12-well plate at an initial density of 17 000 cells per cm^2. They were cultured in hiPSC medium for 6 days with daily change of the medium. Cells were fixed and stained with DAPI and OCT4 antibodies before imaging under the fluorescent microscope.

2.8. Statistical analysis

Results are presented as mean ± standard deviation (SD). Comparison among sorted and unsorted groups was analyzed using ANOVA one-way with post hoc Turkey test (ns: not significant, * p<=0.05, ** p<=0.01, *** p<=0.001).

3. Results

3.1. Differentiation of iPSCs into day 10 SCPCs

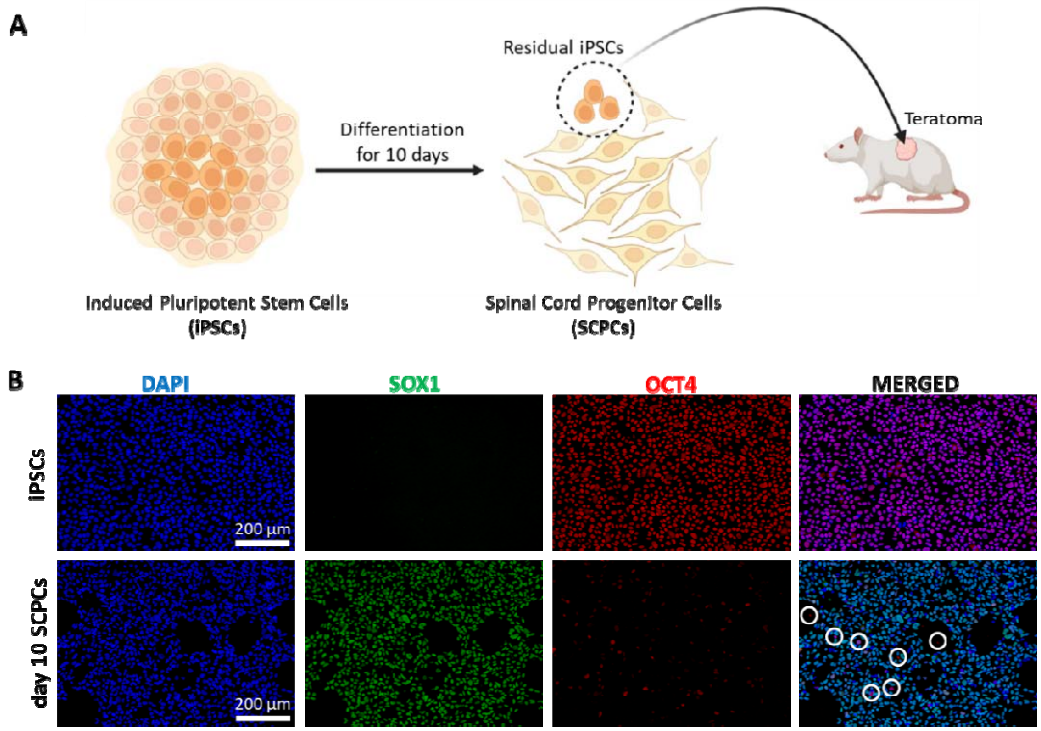

Figure 1 Tumor risk of residual iPSCs in the Spinal Cord Progenitor Cells. (A) iPSCs are differentiated for 10 days to become SCPCs. However, some residual iPSCs in the SCPCs population pose a risk of forming tumors after transplantation (B) Immunofluorescent staining of iPSC and SCPCs at day 10 of differentiation with OCT4 (red), SOX1 (green), and DAPI (blue). In the merged images, some SCPCs (marked by the circles) still express OCT4 but not SOX1.

By mimicking the native development pathway of the spinal cord [25, 26], we generated the SCPCs from iPSCs using 3 small molecules.: ALK inhibitor LDN-193189, GSK3 inhibitor CHIR-99021, and RA. Specifically, neural induction was initiated by adding ALK inhibitor LDN-193189, which inhibits the BMP pathway, and GSK3 inhibitor CHIR-99021, which activates the Wnt pathway. RA was

added to induce caudalization which eventually gives the generated cells a spinal identity. Like other NPCs, the multipotent SCPCs have the potential to differentiate into neurons and glial cells to replace the lost cells in the injured spinal cord. However, the presence of any residual undifferentiated iPSCs has the risk to form teratoma after transplantation (Figure 1B).

The differentiation efficiency of SCPCs on day 10 was assessed based on the expression of pluripotent marker (*i.e.,* OCT4) and neural progenitor marker (*i.e.,* SOX1) in comparison to iPSCs. Previously, we showed that the SCPCs generated using the same protocol gave more than 90 % of SOX1^{+} cells on day 10, which also expressed Nestin and Ki67 [32]. In Figure 1B, iPSCs show a high-level expression of OCT4 and no expression of SOX1. After being differentiated for 10 days, while a majority of SCPCs expressed SOX1, some cells expressed the pluripotent marker OCT4 (marked by the circles), suggesting incomplete differentiation or residual iPSCs.

3.2. Cell size profiling and its correlation with pluripotent biomarker

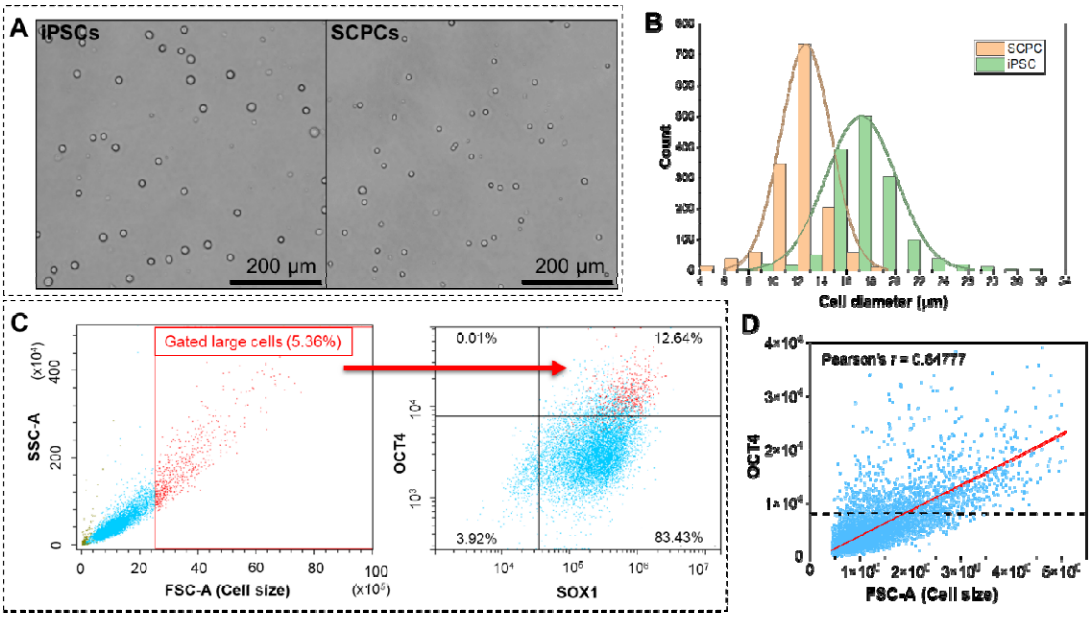

Figure 2 Cell size profiling and its correlation to pluripotent biomarker (OCT4). (A) Microscopy images of suspended iPSCs and SCPCs. (B) Size profiling of the iPSC and SCPC using our customized MATLAB code. (C) Flow cytometer analysis of the SCPCs shows the gated large cells in the SSC-A/FSC-A plot are mostly OCT4-positive cells. (D) Correlation of OCT4 fluorescent intensity with the size of SCPCs. Correlation coefficient Pearson's r = 0.64777. The dashed line gated OCT4 positive and negative cells.

Tracking changes in cell morphology can reveal the efficiency of the differentiation or other intrinsic properties [36]. For example, Jonathan Lin *et al.* built a support vector machine for the classification of the iPSCs and their derivatives based on physical measurements including size,

deformability, deformation kinetics, and morphology with 87.4 % accuracy [37]. According to this study, neural stem cell size was found to be smaller than iPSCs. In our case, the presence of unusually large cells in the SCPCs pool may come from the iPSCs that have not gone through the differentiation. Figure 2A and Figure 2B show the microscopic images and size histograms of the suspended iPSCs and day 10 SCPCs, respectively. It can be seen from the size distribution that SCPCs are more homogeneous with approximately 74% of SCPCs ranging from 10 µm to 14 µm in diameter. Undifferentiated iPSCs, however, are slightly more diverse (*i.e.,* approximately 76 % of iPSCs ranging from 15 µm to 21 µm in diameter) and significantly larger than SCPCs (*i.e.,* their mean difference is 4.5 µm). In flow cytometry, the forward scatter intensity is approximately correlated to cell size and is commonly used for gating cell types of different sizes. By gating out the large SCPCs in the FSC/SSC plot, we found a majority of these cells fall into the $OCT4^+$ position of the OCT4/SOX1 plot (Figure 2C). Moreover, the intensity of OCT4 expression shows a moderate or good correlation to the cell size as shown in Figure 2D with Pearson's correlation of 0.64777. This implies that cell size is positively correlated with OCT4 expression and the residual iPSCs retained their size morphology even after the 10-day differentiation.

3.3. Sized-based separation of SCPCs with the MDDS device

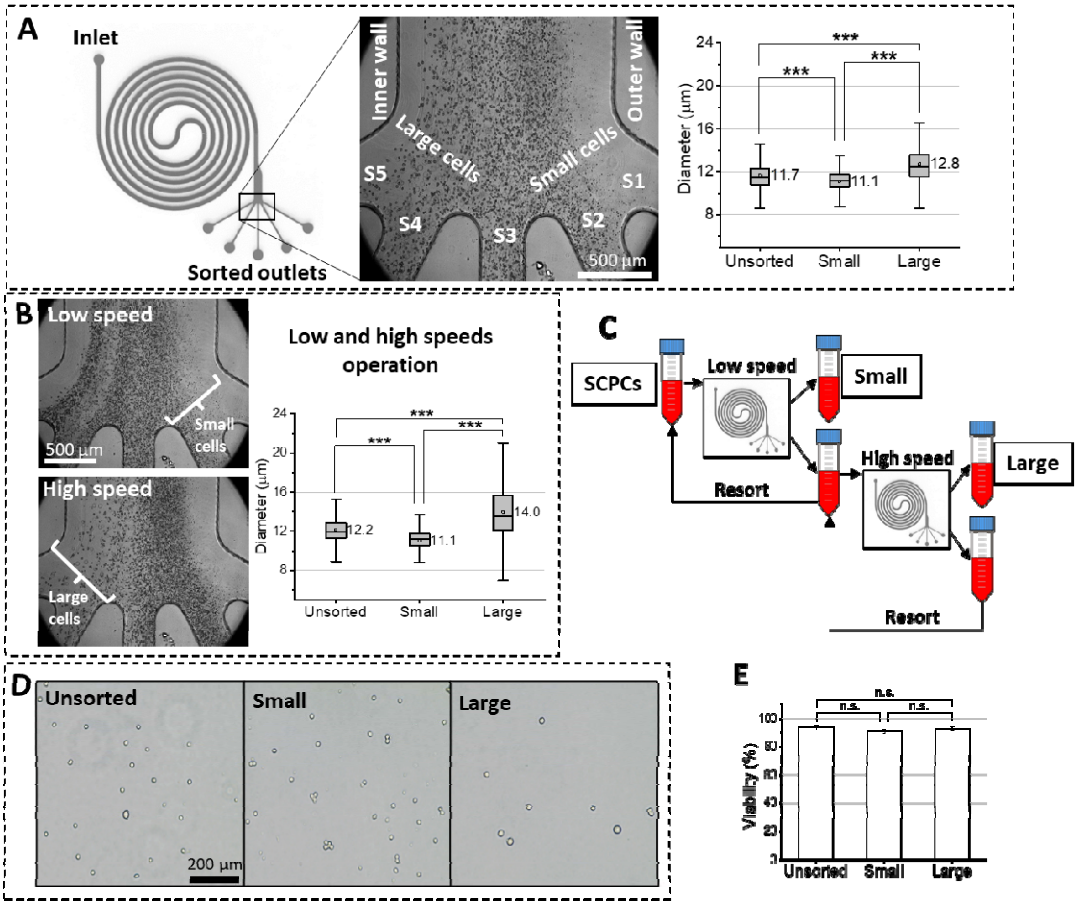

Figure 3 Cell sorting using microfluidic spiral sorter. (A) Working principle of the sorting device. The sample is loaded at the inlet and then goes through the first spiral channel (1) which has a smaller dimension (rectangular cross-section, green-colored channel) for cell focusing, and the second spiral channel (2) has a larger dimension (trapezoidal cross-section, yellow-colored channel) for cell separation [33]. The cells were separated into 5 outlets ranging from the smallest (S1) to the largest (S5). Outlets S1 and S2 were grouped as "Small group", while outlets S4 and S5 were grouped as "Large group". The graph on the right shows the measurement of the cell size of the unsorted group and the sorted small and large groups at the flow rate of 2 mL/min. (B) Low and high speeds operation. A low speed (*i.e.,* 2 mL/min) for collecting small cells and a high speed (*i.e.,* 3 mL/min) for collecting large cells were exploited to increase the separation between small and large groups. The graph shows a better size difference between small and large groups (mean difference of 2.9 µm) compared to the constant speed of 2 ml/min (mean difference of 1.7 µm). (C) A recirculation strategy was used to resort cells that were not collected for both low and high speeds in order to get a sufficient number of cells. (D) Microscopic images of the unsorted and sorted SCPCs in small and large groups using the recirculation method. (E) Viability of the unsorted and sorted SCPCs.

A spiral sorter (MDDS device) was used for size-based sorting of day 10 SCPCs with a high sorting efficiency [33]. As shown in Figure 3A, the device consists of two spiral microfluidic channels with different channel dimensions (see Materials and methods section for details). The device was

tested for its separation of day 10 SCPCs. Initially, cells were sorted into 5 groups corresponding to outlets S1 (smaller cells) to S5 (larger cells). A demonstration of sorting SCPCs spiked with iPSCs and following immunostaining is shown and presented in **Figure S2 of SI**. The results showed S2 group has the lowest OCT4 percentage (~1%) and significantly higher SOX1 and HoxB4 percentages while S4 and S5 contained more iPSCs stained with OCT4. We simplified the experiments by grouping the cells from outlets S1 and S2 as the small group and the cells from outlets S4 and S5 as the large group. It should be noted that outlet S1 contains mostly debris and fragments. The size of unsorted and sorted cells was measured and plotted in the size histogram in Figure 3A. The separation efficiency was not high enough due to the overlap of the sorted groups, so we implemented a high and low speeds operation (Figure 3B), and a recirculation strategy (Figure 3C) for the purpose of increasing the separation efficiency and consistency [38]. When the device is operated at low speed (*e.g.,* 2 mL/min), most of the cells are focused on the inner wall except the very small cells are sorted to outlets S1 and S2 (*i.e.,* small group) due to the Dean drag force. At higher speeds (*e.g.,* 3 mL/min), most of the cells are shifted to the outer wall while the large cells are sorted to outlets S4 and S5 (*i.e.,* large group). Figure 3B shows the size histogram of sorted cell size by using the low and high speeds operation. Compared to the constant sorting speed in Figure 3A, the mean difference between small and large groups was increased from 1.7 µm to 2.9 µm when using the low and high speeds operation. Besides that, a recirculation strategy was also implemented by resorting the uncollected cells to recover more cells to small and large groups (Figure 3C). Cell viability of sorted groups was assessed, and the results showed that cells were highly viable with no significant difference to the unsorted groups.

3.4. Immunofluorescent staining, culture assay, and flow cytometry analysis of sorted day 10 SCOCs

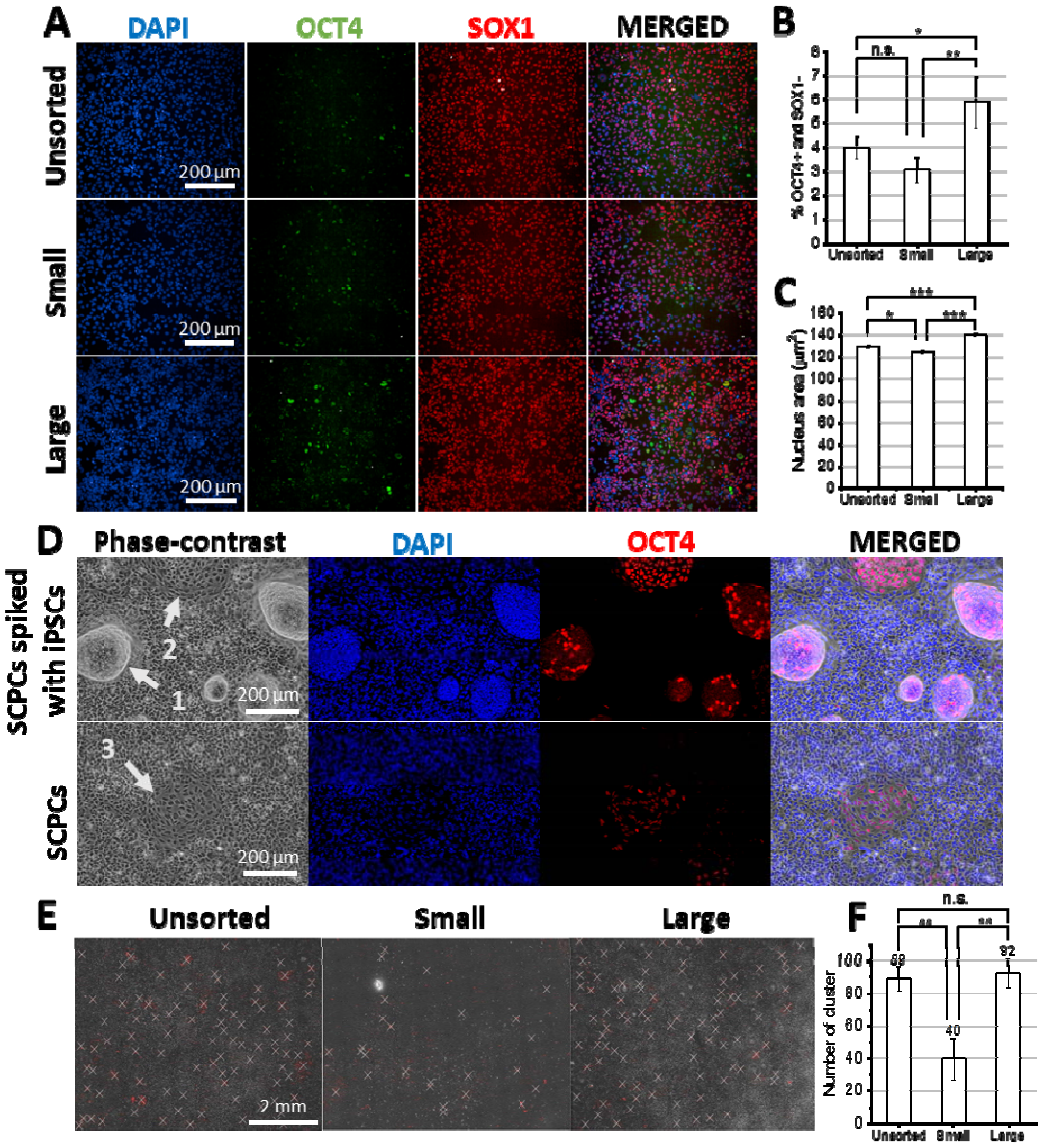

Figure 4 Immunostaining and colony culture assay of sorted CLEC23-SCPCs. CLEC23-SCPCs derived from iPSCs by standard 10-day differentiation protocol. The SCPCs were separated into small and large groups by the inertial device using the recirculation method. (A) Immunofluorescence images of the unsorted group and the sorted small, and large groups of SCPCs with OCT4 (green), SOX1 (red), DAPI (blue), and the merged image (n = 3). (B) Percentage of $OCT4^{+}SOX1^{-}$ cells in the unsorted group and the sorted small, and large groups. (C) Comparison of cell nucleus area between the unsorted group and the sorted small and large groups. (E) Colony culture assay. SCPCs and SCPCs spiked with iPSCs were cultured in an iPSC growth medium on Matrigel coating for 6 days before immunostaining and imaging. The SCPCs spiked with iPSCs were used as a positive control group for the observation of colony morphology formed from spiked iPSCs. Colonies were observed in phase contrast images of both SCPCs and SCPCs spiked with iPSCs. Two types of colony morphology were observed: defined colony (with a sharp edge, compact cells pointed by number 1) and immature colony (with a

defined edge, large nucleus pointed by number 2 for SCPCs spiked iPSCs group and number 3 for SCPCs groups). These colonies were verified by immunofluorescence images with OCT4 (red), DAPI (blue), and the merged image overlaid with phase contrast. (E) Quantification of a colony based on the colocalization of phase contrast and OCT4 staining maps. The map was made of 10 by 10 images. (F) The number of quantified colonies in the unsorted group and the sorted small and large groups (n = 3).

We employed the sorting of SCPCs and characterized the removal efficiency of residual iPSCs. SCPCs were generated by following the normal 10-day differentiation protocol. The collected SCPCs were separated using spiral cell sorters with the recirculation strategy (resorted two times at low speed and three times at high speed, Figure 3C). We compared two separate groups of cells; the small group cells were collected from the outlets S1 and S2, representing the smallest population of SCPCs (therefore potentially representing the highest quality), while the large group cells were collected from outlets S4 and S5, representing the group that is likely rich in residual cells. The three groups (unsorted, small, and large) were stained for immunofluorescent imaging and analysis. While $OCT4^+$ cells were previously considered a marker for potential residual cells in differentiated SCPCs [12], we did not find significant differences in the number of $OCT4^+$ cells among the three groups. However, we found that a subset of $OCT4^+$ cells also expressed SOX1 marker, which could be considered as the cells in the transition stage to be differentiating into SCPCs. Therefore, the cells that expressed OCT4 but not SOX1 (*i.e.,* $OCT4^+SOX1^-$ cells) were analyzed and shown in Figure 4B. It shows the large group had a significantly higher percentage of $OCT4^+SOX1^-$ cells as compared to small and unsorted groups. In terms of nucleus area, cells in the large group show a significantly larger nucleus area than those of unsorted and small groups, consistent with the idea that the nucleus area is a useful marker for differentiating SCPCs and undifferentiated residual iPSCs (Figure 4C).

Previously, a colony culture assay, [39, 40] was used to evaluate the presence of residual undifferentiated cells in cell therapy products. In this assay, the cells were cultured in a culture system, which promotes the growth of iPSCs. We also applied this method to functionally evaluate the level of residual cells in our unsorted and sorted SCPCs. Four separated cell populations, consisting of SCPCs spiked with 13% iPSCs (positive control group), the unsorted SCPCs group, and the sorted small and large SCPCs groups, were cultured in the 12-well plate. Herein, the cells were cultured in iPSC maintenance media for 6 days. Figure 4D shows the colony formation in SCPCs spiked iPSCs group and unsorted SCPCs group. The SCPCs spiked iPSCs group has well-defined colonies with the inner packed cells and sharp edges (pointed by white arrow 1), which are the typical morphologies of iPSC colonies in the culture. The packed and denser cells can also be identified in the DAPI staining image, while the $OCT4^+$ cells are visible in the OCT4 staining image.

Besides the defined colonies, some colonies are yet in their early stages of colony formation with the morphology of the large and elongated nuclei arranged in a circle (pointed by white arrow 2). These immature colonies are stained and confirmed by the OCT4 marker in the immunofluorescent staining. For the unsorted SCPC group, a similar immature colony can also be found with the morphology of a large nuclei arranged in the circle (pointed by white arrow 3). Although immature colonies can be recognized by morphology, some colonies only express OCT4 marker ($OCT4^+$ aggregates) but did not have clear morphologies. Moreover, the distribution of $OCT4^+$ cells in the SCPC group was not always clustered in the form of colonies. Therefore, a density-based method of quantifying $OCT4^+$ cells was developed to quantify the number of forming colonies among unsorted and sorted SCPCs (**Figure S3 in SI**). Quantified colonies in a map of 10 x 10 images are shown in **Figure 4**E. A summary of the counted colonies from the map of different groups is shown in Figure 4F**Error! Reference source not found.Error! Reference source not found.** where unsorted and large groups show a substantially higher number of colonies than the small group. These results indicate that the small group has a much lower chance of forming colonies than unsorted and the large-sized cells.

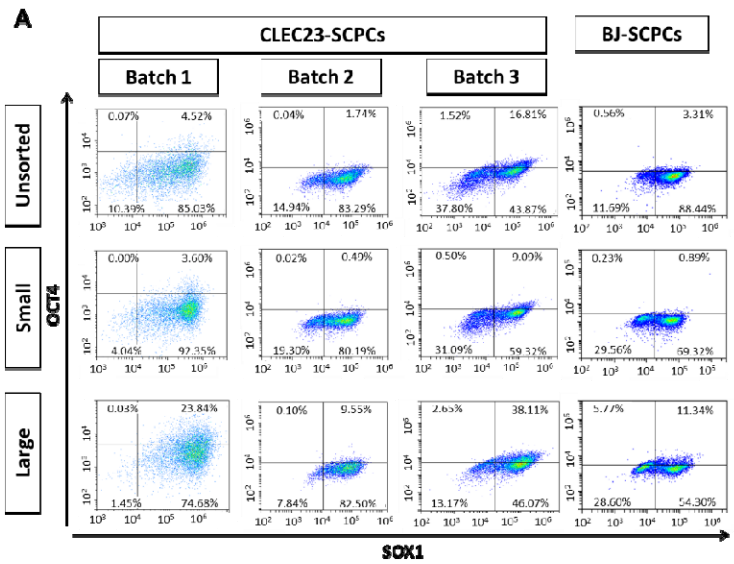

B

% of OCT4+		Unsorted	Small	Large
CLEC23-SCPC	Batch 1	4.59	3.60	23.87
	Batch 2	1.78	0.51	9.65
	Batch 3	18.33	9.59	40.76
BJ-SCPC		3.87	1.12	17.11

C

% of OCT4+ SOX1-		Unsorted	Small	Large
CLEC23-SCPC	Batch 1	0.07	0.00	0.03
	Batch 2	0.04	0.07	0.10
	Batch 3	1.52	0.50	2.65
BJ-SCPC		0.56	0.23	5.77

D

% cell number can be removed		OCT4+	OCT4+SOX1-
CLEC23-SCPC	Batch 1	84.87	7.00
	Batch 2	77.45	35.71
	Batch 3	40.86	37.04
BJ-SCPC		47.08	98.07

Figure 5 Flow cytometry assay to compare $OCT4^+$ percentage of sorted cells from different batches and cell lines. (A) Flow cytometry analysis of the unsorted group and the sorted small and large groups from three batches of day 10 CLEC23-SCPCs generated separately and day 10 BJ-SCPC. Cells were fixed, permeabilized, and stained with OCT4, and SOX1 antibodies labelled with a fluorophore. (B) and (C), the percentage of $OCT4^+$ and $OCT4^+SOX1^-$ cells, respectively, of the unsorted group and the sorted small and large groups. (D) Percentage of $OCT4^+$ and $OCT4^+SOX1^-$ cell numbers can be removed by removing the sorted large group.

Analyzing $OCT4^+$ cells using immunostaining has difficulties of relatively weak expression and errors caused by image-based quantification. On the other hand, flow cytometry is a more common method for the detection of residual undifferentiated cells due to high-speed analysis of a large number of cells (*e.g.*, 100000 cells/second) and the capability of identifying even the minor populations (*i.e.,* $OCT4^+$ cell population) [6, 16, 30]. Especially in this study, forward scatter intensity in the flow cytometer can also give us information about the cell size and its relation to other parameters. Figure 5A shows the dot plot with gated four-quadrant (SOX1 and OCT4) of unsorted and sorted cells from three batches of day 10 CLEC23-SCPCs differentiated separately and day 10 BJ-SCPC. Due to the relatively weak expression level of the OCT4 marker, the percentage of $OCT4^+$ cells was obtained by using fluorescence minus one (FMO) control (*i.e.,* FMO-DAPI-SOX1 control). The $OCT4^+$ percentage of unsorted, sorted small and large groups are presented in Figure 5B. The large group shows from 2-fold to 5-fold increase of $OCT4^+$ cells compared to the unsorted group across different batches and cell lines. Similar to immunostaining results, some of cells among $CT4^+$ SCPCs are also expressing SOX1. While the minority population that expresses OCT4 but not SOX1 would pose a higher risk of forming tumors because they purely expressed pluripotent markers. The percentage of $OCT4^+SOX1^-$ is presented in Figure 5C. It can be seen that batch 3 of CLEC23-SCPCs and BJ-SCPCs show significant higher number of $OCT4^+SOX1^-$ cells. This can be attributed to the higher $OCT4^+$ cells in these groups. For both $OCT4^+$ and $OCT4^+SOX1^-$ quantifications, all small groups showed lower percentage than the unsorted group. Combining with number of sorted cells, number of "tumor-risk" cells (*i.e.,* $OCT4^+$ and $OCT4^+SOX1^-$ cells) can be removed by sorting out the large group is shown in Figure 5D. In general, more than 40% of $OCT4^+$ cells and 30% $OCT4^+SOX1^-$ cells can be removed across different batches and cell lines except for batch 1 of CLEC23-SCPC which has high removal of $OCT4^+$ cells but low removal of $OCT4^+SOX1^-$ cells. Especially, BJ-SCPC can eliminate more than 98% $OCT4^+SOX1^-$ cells. In terms of the expression of iPSC marker, both cell lines show high level of pluripotency (> 98% expressed OCT4, **Figure S5**).

4. Discussion

Due to its self-renewal and tumorigenic traits, residual iPSCs pose a high risk of forming tumors after transplantation. Much research evidence in the past decade have demonstrated tumor formation from residual iPSCs in preclinical studies. Therefore, the removal of residual iPSCs is critical for safe cell therapy. Our study suggested that the large-sized cell group possesses more $OCT4^+$ cells. These signs indicate their similarity to residual iPSCs and implies that residual undifferentiated cells tend to retain their biophysical properties such as size, deformability, or shape during differentiation. By exploiting the size difference between undifferentiated and differentiated cells, we developed a microfluidic size-based sorter for the removal of residual iPSCs in a label-free

and high-throughput manner. Sorted cells were examined with immunofluorescence staining, a culture system for colony formation, and flow cytometry.

Other than cell size, the nucleus area of the cells was significantly decreased during the differentiation. **Figure S1** shows the immunostaining images with DAPI of the iPSCs, and SCPCs differentiated for 4 days and 10 days. By analyzing the nucleus morphology, we found the iPSC nuclei appeared to have a larger nuclei area compared to SCPCs on day 4 and day 10. This is well agreed with the from Figure 4C where large group cells had larger nucleus area than small group cells. The nucleus area could be a good quality attribute for differentiating residual iPSCs in SCPCs or other progenitor cells.

Proliferation assays using EdU with flow cytometry and Ki67 with immunostaining quantifications were also performed on iPSC (day 1) and sorted and unsorted SCPCs on day 10 (**Figure S4**). Compared with SCPCs, iPSCs showed a higher proliferation level owning to unlimited self-renewal of iPSCs. Within SCPC subpopulations, small SCPCs have a lower growth rate than unsorted and large SCPCs. It has previously been suggested that the slow-dividing neural progenitor cells in culture might be better for clinical applications [41]. Meanwhile, hyperproliferative cells (*i.e.,* possibly tumorigenic cells) may be caused by genetic and/or epigenetic transformation of neural progenitor cells, not by the contamination of undifferentiated iPSCs [42, 43]. Regardless of the source of the fast-growing residual cells, the high proliferation of the large group could be associated with higher tumorigenic potential and therefore should be removed to reduce such a risk.

Qualification of stem cells should be mainly discussed in terms of suitability for manufacturing the final products, especially the cell products derived from iPSCs [44]. Our spiral sorter will contribute to the high throughput removal of residual iPSC contaminations. Previously, we demonstrated the sorting throughput of 1L/min corresponding to ~500 million cells/min by using a multiplexed plastic spiral unit containing 100 spiral sorters [45]. Based on the calculation of $OCT4^{+}SOX1^{-}$ percentage from flow cytometry assay and sorted cell number, we can eliminate approximately 32.4% of $OCT4^{+}SOX1^{-}$ cells from day 10 CLEC23-SCPC population and approximately 90.6 % $OCT4^{+}SOX1^{-}$ cells from day 10 BJ-SCPC population by removing the large group (Figure 5D). While the method works for different iPSC lines, the differences in size distribution and differentiation efficiency also validated that the differentiation might not be fully efficient and can be cell origin dependent [46-48].

Overall, our device takes advantage of the size differences between the undifferentiated and differentiated cells to enrich the SCPCs population while reducing the percentage of iPSCs. The technology is also label-free, non-contact, and has high throughput without affecting cell viability

and functions. Further development of this technology will be promising for the cell manufacturing workflow, contributing to better quality and safety of the transplanted cells by reducing the number of potentially tumor-forming cells.

5. Acknowledgments

This research was supported by National Research Foundation, Singapore, under its Intra-CREATE Thematic Grant (Award number: NRF2019-THE002-0001) and Campus for Research Excellence and Technological Enterprise (CREATE) programme, through Singapore MIT Alliance for Research and Technology (SMART): Critical Analytics for Manufacturing Personalised-Medicine (CAMP) Inter-Disciplinary Research Group.

6. References

1. Takahashi, K. and S. Yamanaka, *Induction of Pluripotent Stem Cells from Mouse Embryonic and Adult Fibroblast Cultures by Defined Factors.* Cell, 2006. **126**(4): p. 663-676.
2. Hong, So G., et al., *Path to the Clinic: Assessment of iPSC-Based Cell Therapies In Vivo in a Nonhuman Primate Model.* Cell Reports, 2014. **7**(4): p. 1298-1309.
3. Yasuda, S., et al., *Tumorigenicity-associated characteristics of human iPS cell lines.* PLOS ONE, 2018. **13**(10): p. e0205022.
4. Yasuda, S. and Y. Sato, *Tumorigenicity assessment of human cell-processed therapeutic products.* Biologicals, 2015. **43**(5): p. 416-421.
5. Zhang, Y., et al., *Intramyocardial Transplantation of Undifferentiated Rat Induced Pluripotent Stem Cells Causes Tumorigenesis in the Heart.* PLOS ONE, 2011. **6**(4): p. e19012.
6. *Residual Undifferentiated Cells During Differentiation of Induced Pluripotent Stem Cells In Vitro and In Vivo.* Stem Cells and Development, 2012. **21**(4): p. 521-529.
7. Gropp, M., et al., *Standardization of the Teratoma Assay for Analysis of Pluripotency of Human ES Cells and Biosafety of Their Differentiated Progeny.* PLOS ONE, 2012. **7**(9): p. e45532.
8. Ben-David, U. and N. Benvenisty, *The tumorigenicity of human embryonic and induced pluripotent stem cells.* Nature Reviews Cancer, 2011. **11**(4): p. 268-277.
9. Gutierrez-Aranda, I., et al., *Human Induced Pluripotent Stem Cells Develop Teratoma More Efficiently and Faster Than Human Embryonic Stem Cells Regardless the Site of Injection.* Stem Cells, 2010. **28**(9): p. 1568-1570.
10. Lee, A.S., et al., *Tumorigenicity as a clinical hurdle for pluripotent stem cell therapies.* Nature Medicine, 2013. **19**(8): p. 998-1004.
11. Garitaonandia, I., et al., *Neural Stem Cell Tumorigenicity and Biodistribution Assessment for Phase I Clinical Trial in Parkinson's Disease.* Scientific Reports, 2016. **6**(1): p. 34478.
12. Sugai, K., et al., *First-in-human clinical trial of transplantation of iPSC-derived NS/PCs in subacute complete spinal cord injury: Study protocol.* Regenerative Therapy, 2021. **18**: p. 321-333.
13. *Selective Removal of Undifferentiated Human Embryonic Stem Cells Using Magnetic Activated Cell Sorting Followed by a Cytotoxic Antibody.* Tissue Engineering Part A, 2012. **18**(9-10): p. 899-909.
14. Tan, H.L., et al., *mAb 84, a Cytotoxic Antibody that Kills Undifferentiated Human Embryonic Stem Cells via Oncosis.* Stem Cells, 2009. **27**(8): p. 1792-1801.

15. Lim, D.Y.X., et al., *Cytotoxic antibody fragments for eliminating undifferentiated human embryonic stem cells.* Journal of Biotechnology, 2011. **153**(3): p. 77-85.
16. Fong, C.Y., et al., *Separation of SSEA-4 and TRA-1–60 Labelled Undifferentiated Human Embryonic Stem Cells from A Heterogeneous Cell Population Using Magnetic-Activated Cell Sorting (MACS) and Fluorescence-Activated Cell Sorting (FACS).* Stem Cell Reviews and Reports, 2009. **5**(1): p. 72-80.
17. Ben-David, U., et al., *Selective Elimination of Human Pluripotent Stem Cells by an Oleate Synthesis Inhibitor Discovered in a High-Throughput Screen.* Cell Stem Cell, 2013. **12**(2): p. 167-179.
18. Tang, C., et al., *An antibody against SSEA-5 glycan on human pluripotent stem cells enables removal of teratoma-forming cells.* Nature Biotechnology, 2011. **29**(9): p. 829-834.
19. Haramoto, Y., et al., *A technique for removing tumourigenic pluripotent stem cells using rBC2LCN lectin.* Regenerative Therapy, 2020. **14**: p. 306-314.
20. Onuma, Y., et al., *rBC2LCN, a new probe for live cell imaging of human pluripotent stem cells.* Biochemical and Biophysical Research Communications, 2013. **431**(3): p. 524-529.
21. Lin, Y.-T., et al., *Elimination of undifferentiated human embryonic stem cells by cardiac glycosides.* Scientific Reports, 2017. **7**(1): p. 5289.
22. Lee, M.-O., et al., *Inhibition of pluripotent stem cell-derived teratoma formation by small molecules.* Proceedings of the National Academy of Sciences, 2013. **110**(35): p. E3281-E3290.
23. Curtis, E., et al., *A First-in-Human, Phase I Study of Neural Stem Cell Transplantation for Chronic Spinal Cord Injury.* Cell Stem Cell, 2018. **22**(6): p. 941-950.e6.
24. Cusimano, M., et al., *Transplanted neural stem/precursor cells instruct phagocytes and reduce secondary tissue damage in the injured spinal cord.* Brain, 2012. **135**(2): p. 447-460.
25. Kumamaru, H., et al., *Generation and post-injury integration of human spinal cord neural stem cells.* Nat Methods, 2018. **15**(9): p. 723-731.
26. Kajikawa, K., et al., *Cell therapy for spinal cord injury by using human iPSC-derived region-specific neural progenitor cells.* Mol Brain, 2020. **13**(1): p. 120.
27. Dell'Anno, M.T., et al., *Human neuroepithelial stem cell regional specificity enables spinal cord repair through a relay circuit.* Nat Commun, 2018. **9**(1): p. 3419.
28. Lim, R.H.G., et al., *Safety Evaluation of Human Cord-Lining Epithelial Stem Cells Transplantation for Liver Regeneration in a Porcine Model.* Cell Transplant, 2020. **29**: p. 963689719896559.
29. Saleh, R. and H.M. Reza, *Short review on human umbilical cord lining epithelial cells and their potential clinical applications.* Stem Cell Research & Therapy, 2017. **8**(1): p. 222.
30. Kuroda, T., et al., *Highly Sensitive In Vitro Methods for Detection of Residual Undifferentiated Cells in Retinal Pigment Epithelial Cells Derived from Human iPS Cells.* PLOS ONE, 2012. **7**(5): p. e37342.
31. Hor, J.H., et al., *Cell cycle inhibitors protect motor neurons in an organoid model of Spinal Muscular Atrophy.* Cell Death Dis, 2018. **9**(11): p. 1100.
32. Winanto, et al., *Organoid cultures of MELAS neural cells reveal hyperactive Notch signaling that impacts neurodevelopment.* Cell Death Dis, 2020. **11**(3): p. 182.
33. Jeon, H., et al., *Fully-automated and field-deployable blood leukocyte separation platform using multi-dimensional double spiral (MDDS) inertial microfluidics.* Lab on a Chip, 2020. **20**(19): p. 3612-3624.
34. Jeon, H., et al., *Fully Automated, Sample-to-Answer Leukocyte Functional Assessment Platform for Continuous Sepsis Monitoring via Microliters of Blood.* ACS Sensors, 2021. **6**(7): p. 2747-2756.
35. Jeon, H., et al., *Multi-dimensional-double-spiral (MDDS) inertial microfluidic platform for sperm isolation directly from the raw semen sample.* Scientific Reports, 2022. **12**(1): p. 4212.
36. Darling, E.M. and D.D. Carlo, *High-Throughput Assessment of Cellular Mechanical Properties.* Annual Review of Biomedical Engineering, 2015. **17**(1): p. 35-62.

37. Lin, J., et al., *High-throughput physical phenotyping of cell differentiation.* Microsystems & Nanoengineering, 2017. **3**(1): p. 17013.
38. Ryu, H., et al., *Patient-Derived Airway Secretion Dissociation Technique To Isolate and Concentrate Immune Cells Using Closed-Loop Inertial Microfluidics.* Analytical Chemistry, 2017. **89**(10): p. 5549-5556.
39. Tano, K., et al., *A Novel In Vitro Method for Detecting Undifferentiated Human Pluripotent Stem Cells as Impurities in Cell Therapy Products Using a Highly Efficient Culture System.* PLOS ONE, 2014. **9**(10): p. e110496.
40. Watanabe, T., et al., *Multisite studies for validation and improvement of a highly efficient culture assay for detection of undifferentiated human pluripotent stem cells intermingled in cell therapy products.* Cytotherapy, 2021. **23**(2): p. 176-183.
41. Furutachi, S., et al., *Slowly dividing neural progenitors are an embryonic origin of adult neural stem cells.* Nature Neuroscience, 2015. **18**(5): p. 657-665.
42. Sugai, K., et al., *Pathological classification of human iPSC-derived neural stem/progenitor cells towards safety assessment of transplantation therapy for CNS diseases.* Molecular Brain, 2016. **9**(1): p. 85.
43. Iida, T., et al., *Whole-Genome DNA Methylation Analyses Revealed Epigenetic Instability in Tumorigenic Human iPS Cell-Derived Neural Stem/Progenitor Cells.* Stem Cells, 2017. **35**(5): p. 1316-1327.
44. Jha, B.S., M. Farnoodian, and K. Bharti, *Regulatory considerations for developing a phase I investigational new drug application for autologous induced pluripotent stem cells-based therapy product.* STEM CELLS Translational Medicine, 2021. **10**(2): p. 198-208.
45. Jeon, H., et al., *Engineering a deformation-free plastic spiral inertial microfluidic system for CHO cell clarification in biomanufacturing.* Lab on a Chip, 2022. **22**(2): p. 272-285.
46. Hu, B.-Y., et al., *Neural differentiation of human induced pluripotent stem cells follows developmental principles but with variable potency.* Proceedings of the National Academy of Sciences, 2010. **107**(9): p. 4335-4340.
47. Strano, A., et al., *Variable Outcomes in Neural Differentiation of Human PSCs Arise from Intrinsic Differences in Developmental Signaling Pathways.* Cell Reports, 2020. **31**(10).
48. Hargus, G., et al., *Origin-Dependent Neural Cell Identities in Differentiated Human iPSCs In Vitro and after Transplantation into the Mouse Brain.* Cell Reports, 2014. **8**(6): p. 1697-1703.

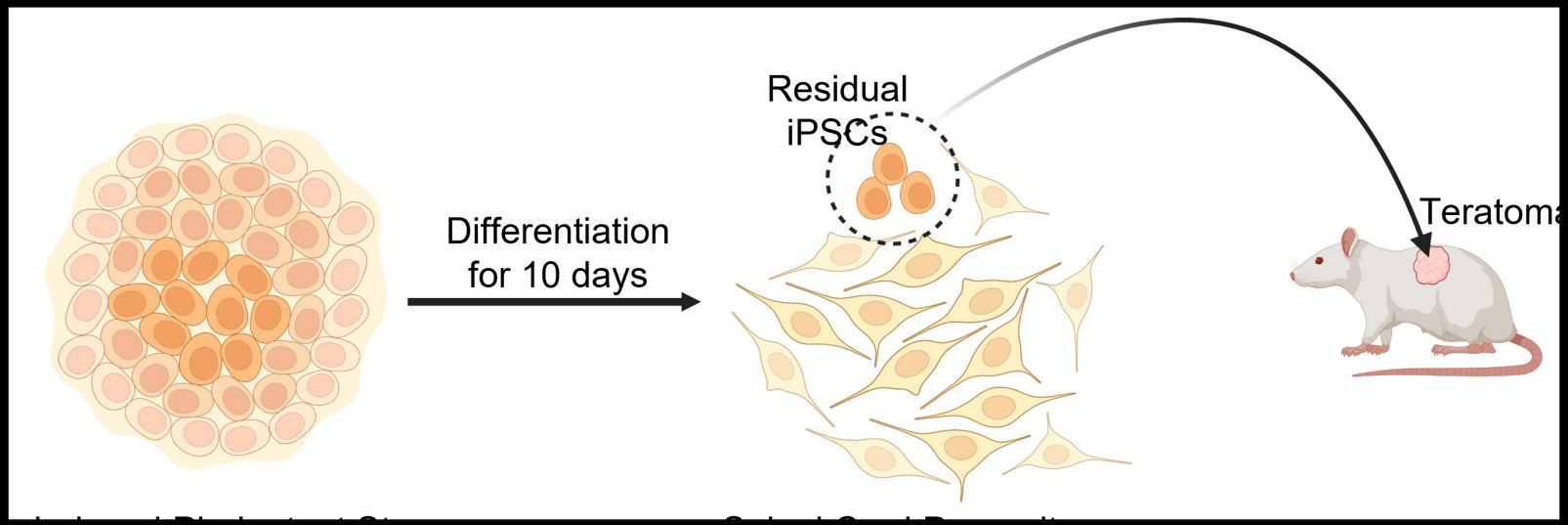
Differentiation
for 10 days
Residual
iPSCs
Teratoma

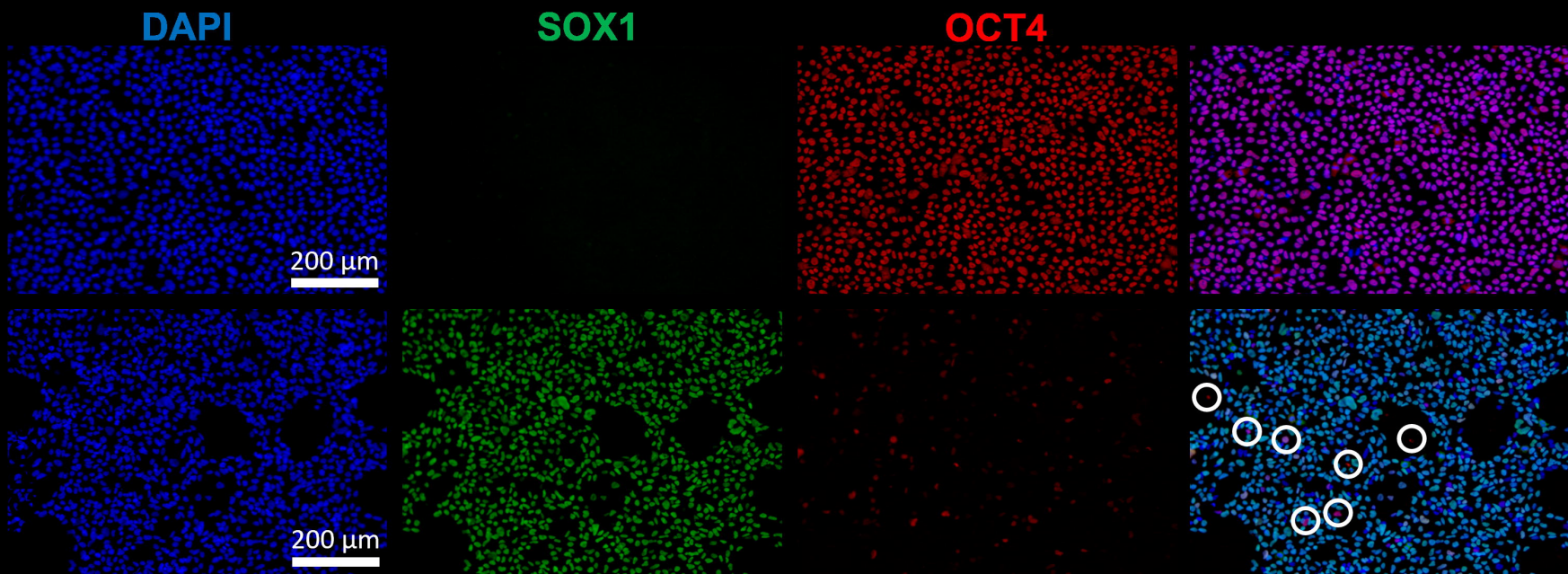
DAPI
SOX1
OCT4
200 µm
200 µm

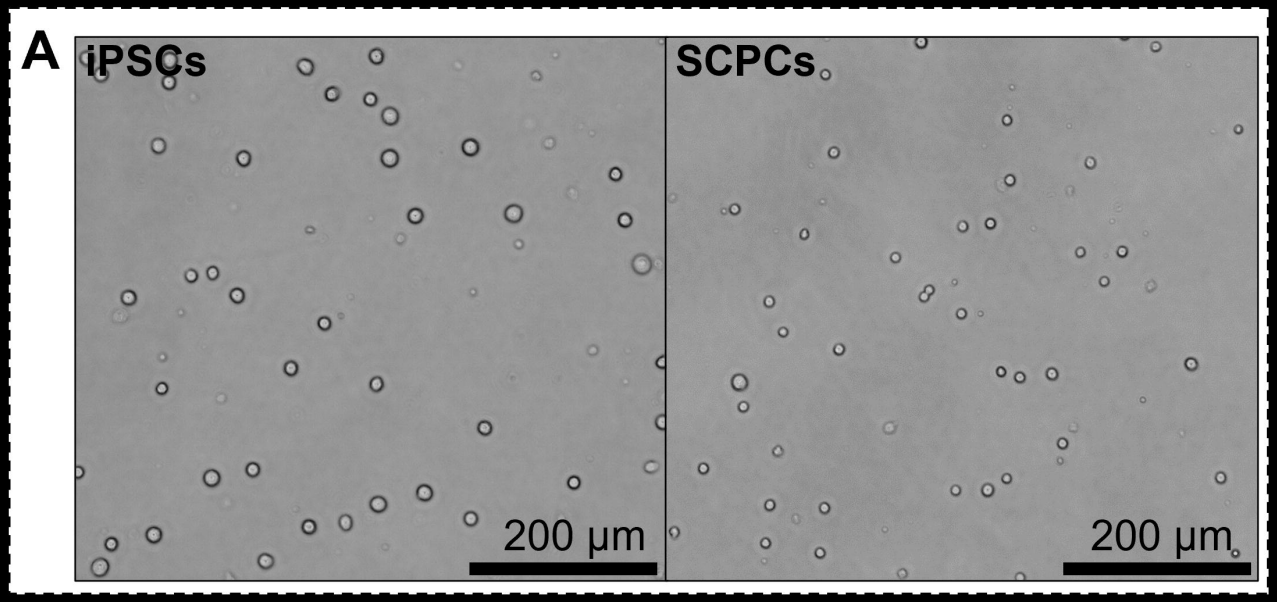
A
iPSCs
SCPCs
200 µm
200 µm

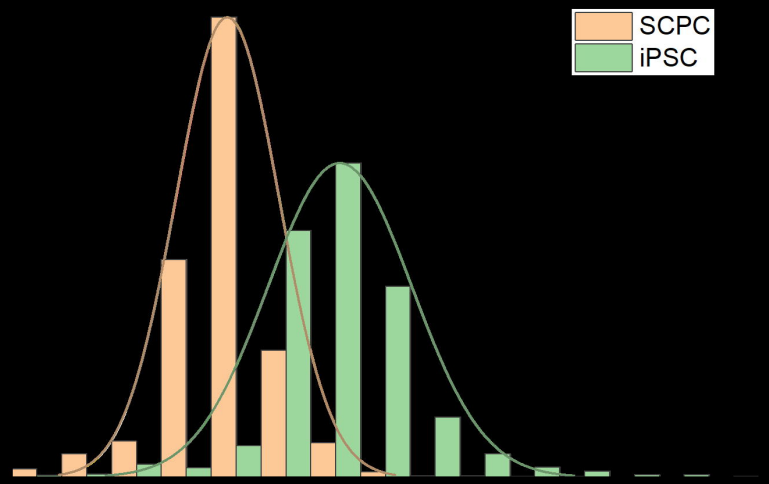
SCPC
iPSC

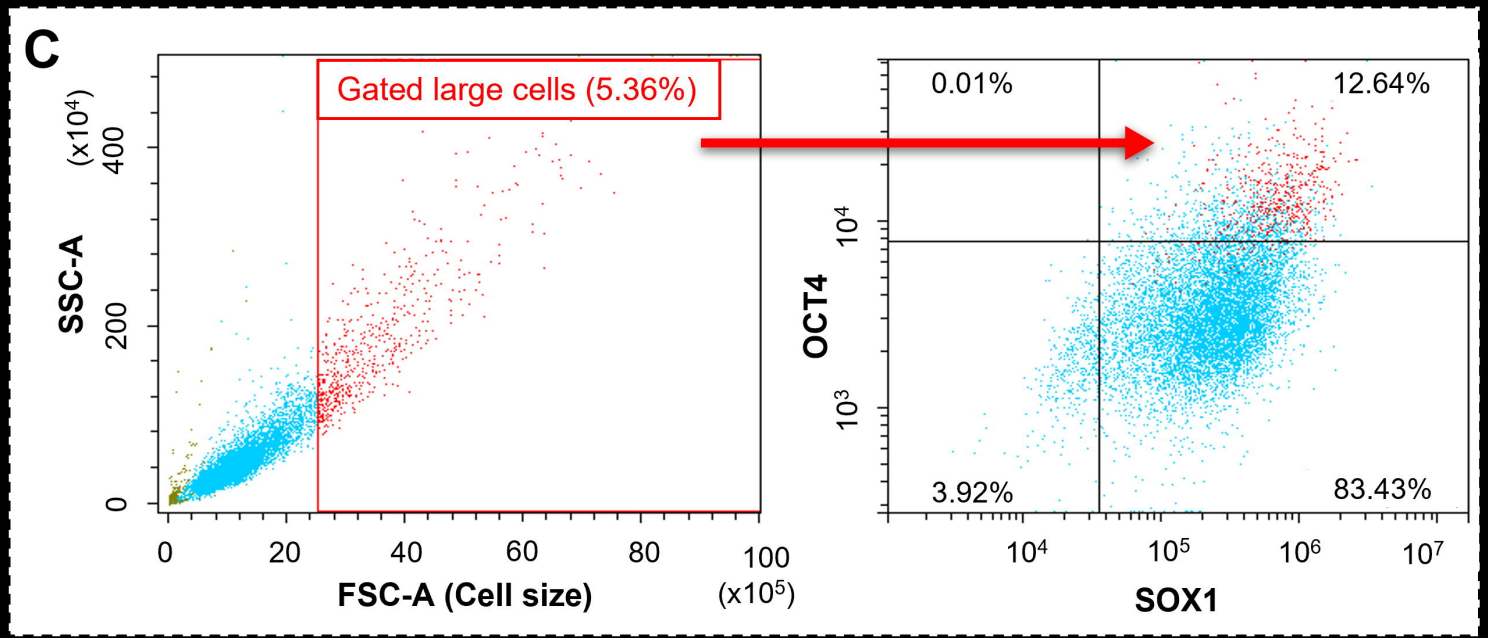
C
Gated large cells (5.36%)
SSC-A
(x10⁴)
400
200
0
0
20
40
60
80
100
(x10⁵)
FSC-A (Cell size)
0.01%
12.64%
3.92%
83.43%
OCT4
10⁴
10³
10⁴
10⁵
10⁶
10⁷
SOX1

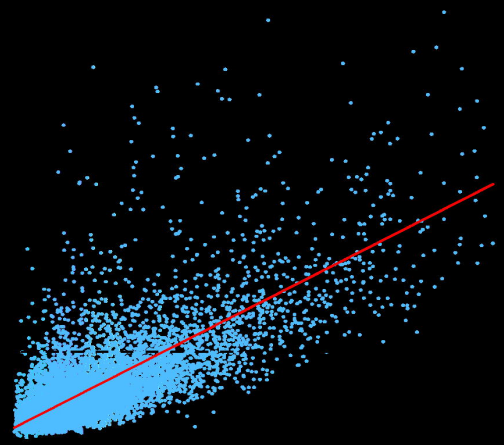

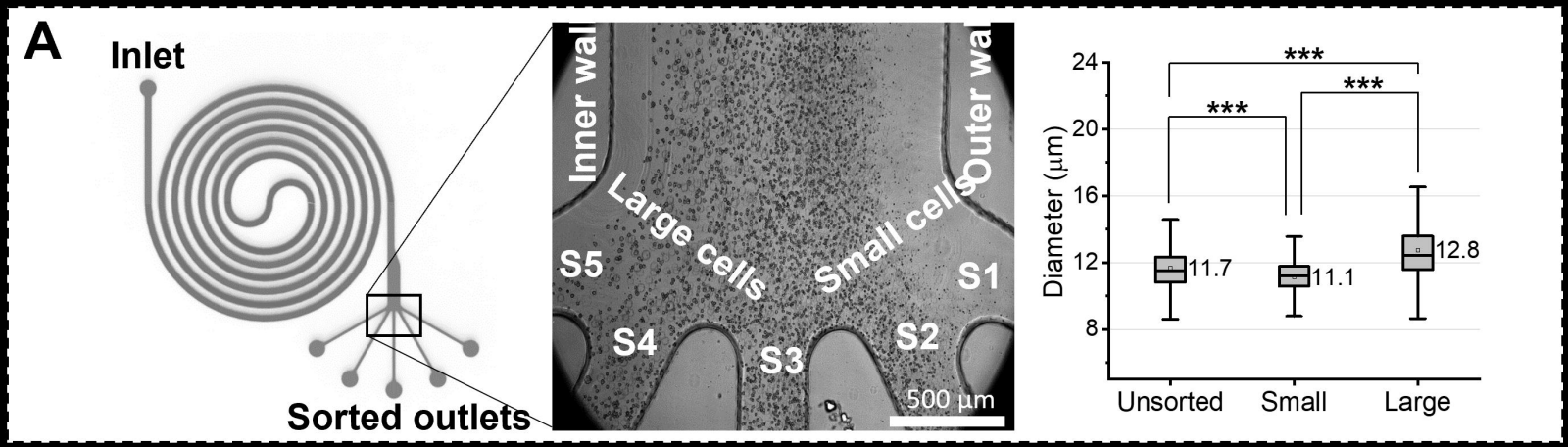
A
Inlet
Sorted outlets
Inner wall
Outer wall
Large cells
Small cells
S5
S1
S4
S3
S2
500 µm
Diameter (µm)
24
20
16
12
8
***
***
***
11.7
11.1
12.8
Unsorted
Small
Large

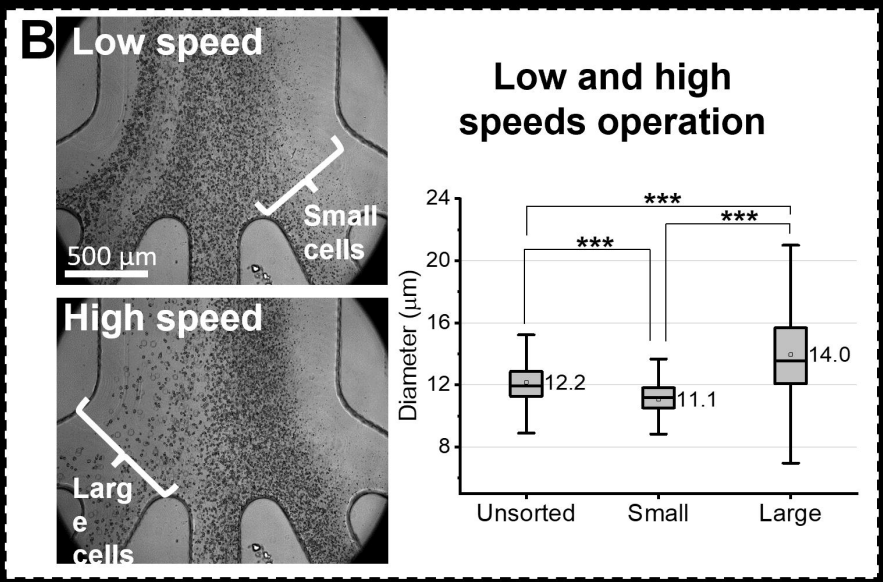
B
Low speed
Small cells
500 µm
High speed
Large cells
Low and high speeds operation
Diameter (µm)
24
20
16
12
8
***
***
***
12.2
11.1
14.0
Unsorted
Small
Large

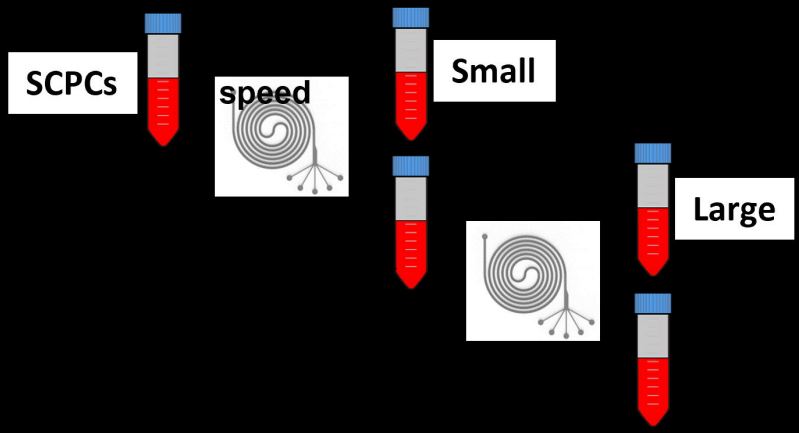
SCPCs
speed
Small
Large

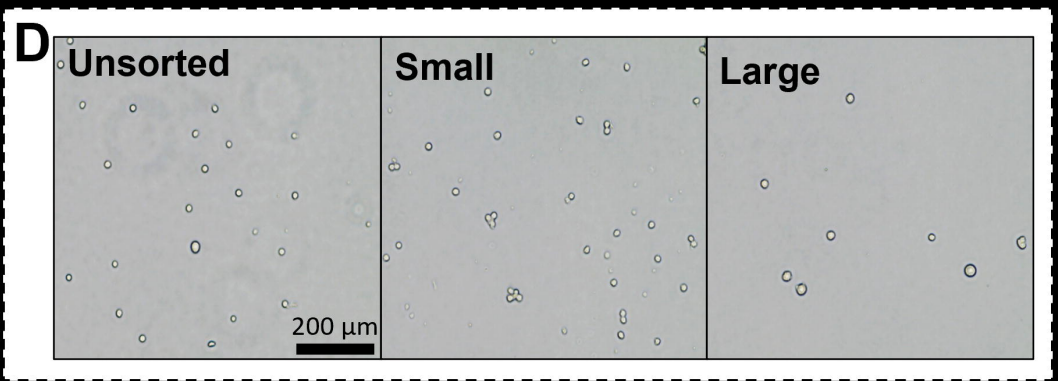
D
Unsorted
Small
Large
200 µm

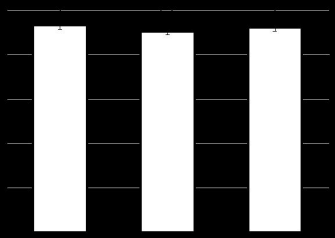

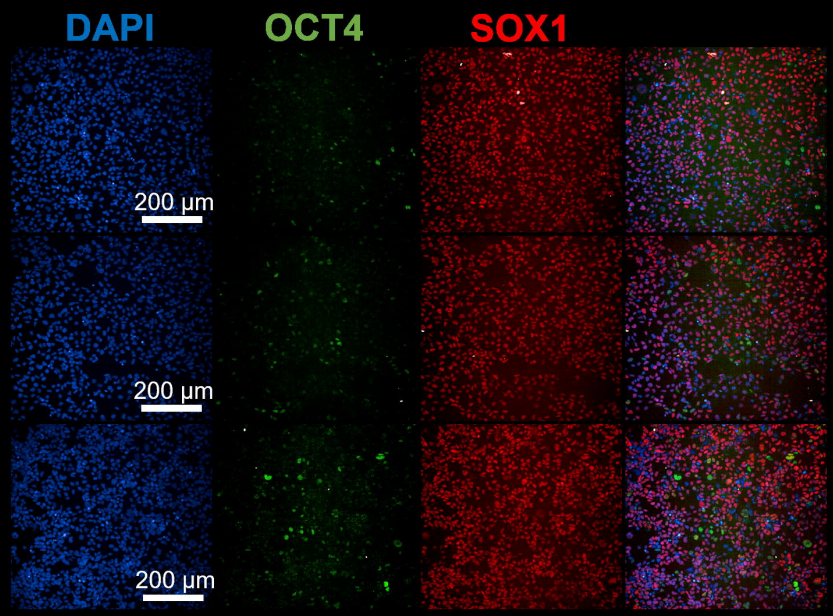
DAPI
OCT4
SOX1
200 µm
200 µm
200 µm

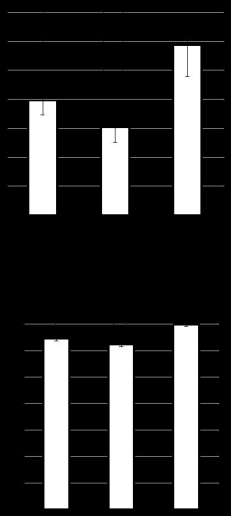

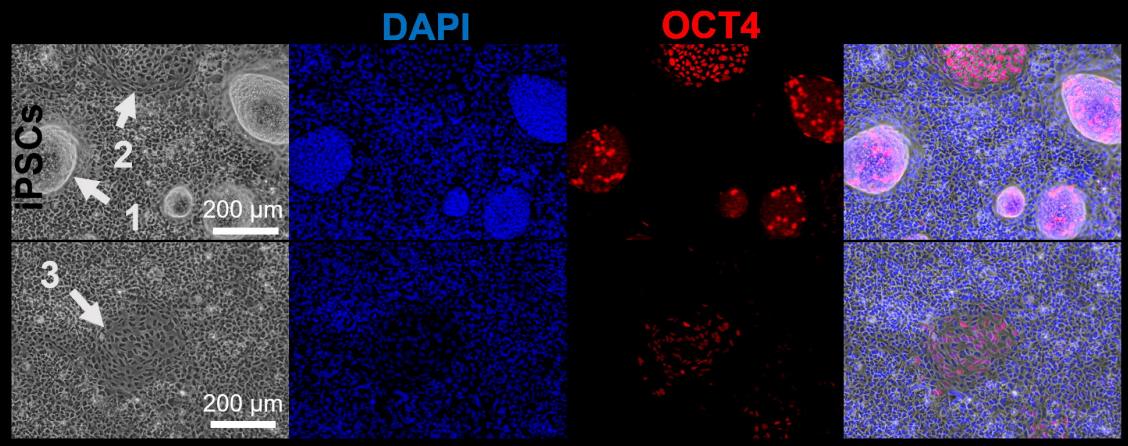
DAPI
OCT4
iPSCs
2
1
3
200 µm
200 µm

2 mm

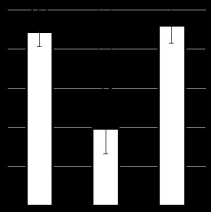

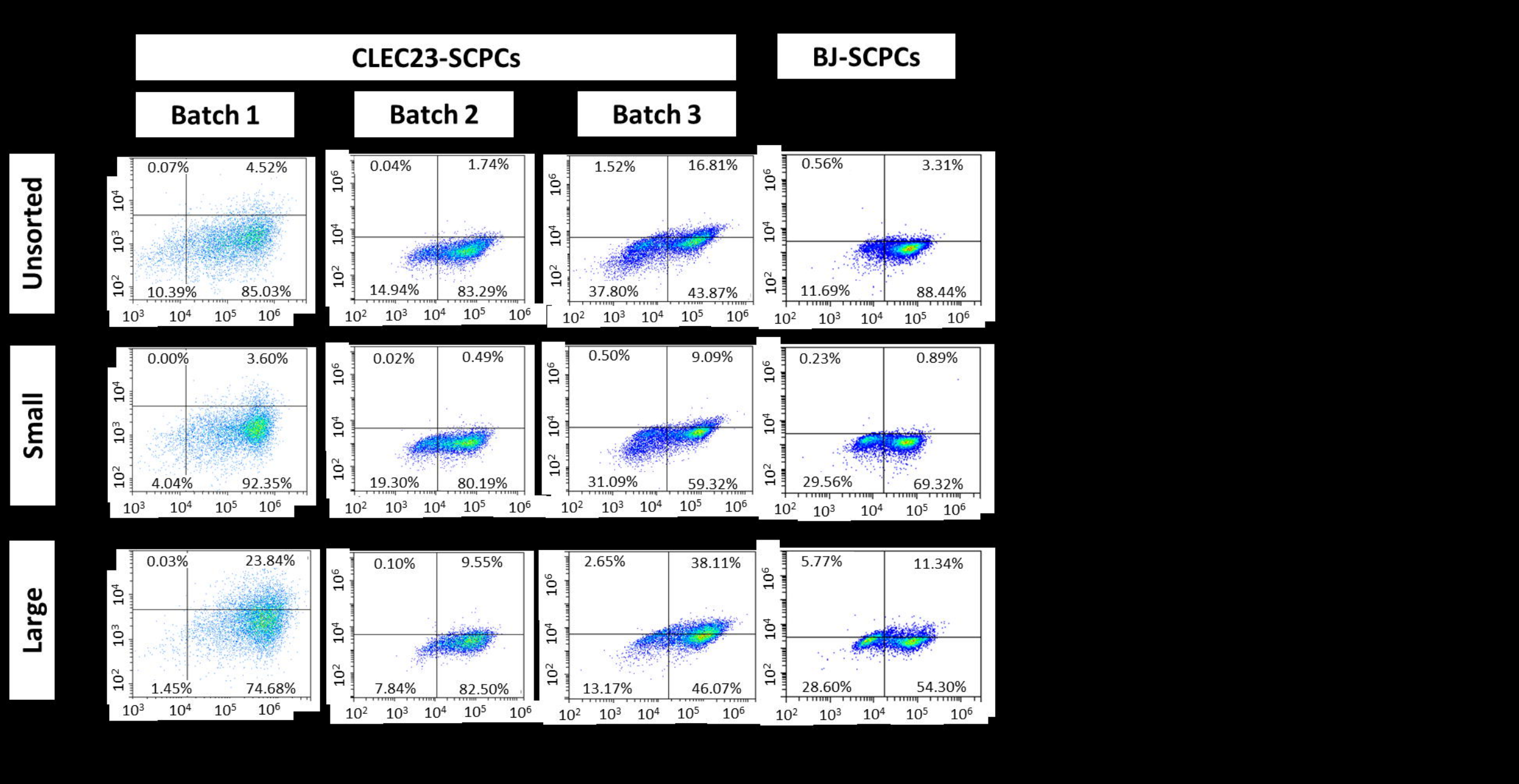
CLEC23-SCPCs
BJ-SCPCs
Batch 1
Batch 2
Batch 3
Unsorted
Small
Large
0.07%
4.52%
10.39%
85.03%
0.04%
1.74%
14.94%
83.29%
1.52%
16.81%
37.80%
43.87%
0.56%
3.31%
11.69%
88.44%
0.00%
3.60%
4.04%
92.35%
0.02%
0.49%
19.30%
80.19%
0.50%
9.09%
31.09%
59.32%
0.23%
0.89%
29.56%
69.32%
0.03%
23.84%
1.45%
74.68%
0.10%
9.55%
7.84%
82.50%
2.65%
38.11%
13.17%
46.07%
5.77%
11.34%
28.60%
54.30%